Article

Observation of MLCT and MLCT Excited States in Quadruply Bonded Mo and W Complexes

Matthew J. Byrnes, Malcolm H. Chisholm, Judith A. Gallucci, Yao Liu, Ramkrishna Ramnauth, and Claudia Turro

J. Am. Chem. Soc., **2005**, 127 (49), 17343-17352• DOI: 10.1021/ja055136h • Publication Date (Web): 12 November 2005

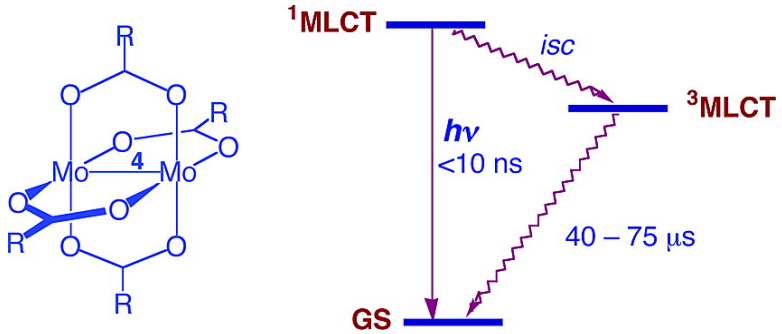

More About This Article

Additional resources and features associated with this article are available within the HTML version:

- Supporting Information
- Links to the 6 articles that cite this article, as of the time of this article download
- Access to high resolution figures
- Links to articles and content related to this article
- Copyright permission to reproduce figures and/or text from this article

View the Full Text HTML

J|A|C|S
ARTICLES
Published on Web 11/12/2005

Observation of ^{1}MLCT and ^{3}MLCT Excited States in Quadruply Bonded Mo_2 and W_2 Complexes

Matthew J. Byrnes, Malcolm H. Chisholm,* Judith A. Gallucci, Yao Liu, Ramkrishna Ramnauth, and Claudia Turro*

Contribution from the Department of Chemistry, The Ohio State University, 100 West 18th Avenue, Columbus, Ohio 43210-1185

Received July 28, 2005; E-mail: chisholm@chemistry.ohio-state.edu; turro@chemistry.ohio-state.edu

Abstract: The photophysical properties of the series of quadruply bonded $M_2(O_2C-Ar)_4$ [M = Mo, Ar = phenyl (ph), 1-naphthalene (1-nap), 2-naphthalene (2-nap), 9-anthracene (9-an), 1-pyrene (1-py), and 2-pyrene (2-py); M = W, Ar = ph, 2-nap] complexes were investigated. The lowest energy absorption of the complexes is attributed to a metal-to-ligand charge transfer ^{1}MLCT transition from the metal-based δ HOMO to the π^* O_2C-Ar LUMO. The $Mo_2(O_2C-Ar)_4$ complexes exhibit weak short-lived emission (<10 ns) and a nonemissive, long-lived (40−76 μs) excited state detected by transient absorption spectroscopy. The short- and long-lived species are attributed to the ^{1}MLCT and ^{3}MLCT excited states, respectively, based on the large Stokes shift, vibronic progression in the low-temperature emission spectrum, and solvent dependence. Comparisons are made to the $W_2(O_2C-Ar)_4$ complexes, which are easier to oxidize and exhibit greater spin−orbit coupling than the Mo_2 systems. From the excited-state energy of the emissive ^{1}MLCT state and the electrochemical properties of the complexes, it is predicted that this excited state should be a powerful reducing agent. The crystal and molecular structure of $Mo_2(O_2C-9\text{-an})_4$ is also reported together with electronic structure calculations employing density functional theory. To our knowledge, this is the first observation of MLCT excited states in quadruply bonded complexes. In addition, the photophysical properties of the present systems parallel those of organic aromatic molecules and may be viewed as metal-mediated organics. The introduction of the M_2 δ^* orbital in the complexes in conjugation with the organic π-system of the ligands affords the opportunity to tune the excited-state energies and redox potentials.

Introduction

The photophysical properties and photoinduced reactivity of $[Ru(bpy)_3]^{2+}$ (bpy = 2,2′-bipyridine) and related mononuclear octahedral complexes have been investigated extensively owing to the potential applications of their emissive, long-lived ^{3}MLCT (metal-to-ligand charge transfer) excited states.[1,2] In particular, the ability of the ^{3}MLCT excited state to transfer energy to various substrates and to act as both a reducing and oxidizing agent continues to place these complexes as potential agents in various applications, including their use as sensitizers in polymer photocells,[3,4] in the study of long-range charge transfer in biological systems[5−7] and in photodynamic therapy.[8,9]

Since the lowest energy absorption in the quadruply bonded bimetallic tetracarboxylate complexes of the type $Mo_2(O_2C-Ar)_4$ (M = Mo, W; Ar = aromatic or fused aromatic ring) has been previously shown to be MLCT in nature,[10] it is possible that a long-lived ^{3}MLCT excited state similar to that in $[Ru(bpy)_3]^{2+}$ is also present in these systems, which may possess similar or improved photophysical properties and photoreactivity. The $Mo_2(O_2C-Ar)_4$ quadruply bonded complexes exhibit metal-centered electron configurations Mo_2 $\sigma^2\pi^4\delta^2$, with aryl carboxylate π^* as the lowest unoccupied molecular orbital (LUMO). The strong absorption in the visble region observed for $Mo_2(O_2C-Ar)_4$ and related complexes has been assigned as $(Mo_2\ \delta)^2\ (O_2C-Ar\ \pi^*)^0 \rightarrow (Mo_2\ \delta)^1\ (O_2C-Ar\ \pi^*)^1$, which represents a spin-allowed ^{1}MLCT transition from the bimetallic core to the aryl carboxylate ligands. As was previously shown by the Chisholm group for quadruply bonded Mo_2 complexes possessing thienyl carboxylate bridging ligands, the MLCT absorption can be very intense ($\epsilon \sim 50\,000\ M^{-1}\ cm^{-1}$) and the maximum can be tuned to span the entire visible region of the spectrum.[11]

The potential for the presence of an MLCT excited state in the $Mo_2(O_2C-Ar)_4$ complexes is unprecedented in quadruply bonded complexes. The short-lived luminescence from Mo_2^{4+}

(1) Meyer, T. J. *Acc. Chem. Res.* **1989**, *22*, 163.
(2) Juris, A.; Balzani, V.; Barigelletti, F.; Campagna, S.; Belser, P.; von Zelewsky, A. *Coord. Chem. Rev.* **1988**, *84*, 85.
(3) Kalyanasundaram, K.; Gratzel, M. *Coord. Chem. Rev.* **1998**, *177*, 347.
(4) Saito, Y.; Azechi, T.; Kitamura, T.; Hasegawa, Y.; Wada, Y.; Yanagida, S. *Coord. Chem. Rev.* **2004**, *248*, 1469.
(5) Berglund, J.; Pascher, T.; Winkler, J. R.; Gray, H. B. *J. Am. Chem. Soc.* **1997**, *119*, 2464.
(6) Wuttke, D. S.; Bjerrum, M. J.; Winkler, J. R.; Gray, H. B. *Science* **1992**, *256*, 1007.
(7) Beratan, D. N.; Onuchic, J. N.; Winkler, J. R.; Gray, H. B. *Science* **1992**, *258*, 1740.
(8) Clarke, M. J. *Coord. Chem. Rev.* **2003**, *236*, 209.
(9) DeRosa, M. C.; Crutchley, R. J. *Coord. Chem. Rev.* **2002**, *233−234*, 351.
(10) Cotton, F. A.; Walton, R. A. *Multiple Bonds between Metal Atoms*, 2nd ed.; Oxford University Press: New York, 1993.
(11) Byrnes, M. J.; Chisholm, M. H.; Clark, R. J. H.; Gallucci, J. C.; Hadad, C. M.; Patmore, N. J. *Inorg. Chem.* **2004**, *43*, 6334.

and related systems observed to date arises from a metal-centered $^1\delta\delta^*$ excited state.[12,13] Although the photochemistry of certain Mo_2^{4+} systems has been investigated for potential applications in redox catalysis, the short lifetime of the $^1\delta\delta^*$ excited states precludes efficient bimolecular reactivity.[14,15] To begin the exploration of the photophysical properties of aryl carboxylate-bridged Mo_2^{4+} compounds, the series $M_2(O_2C-Ar)_4$ [M = Mo, Ar = phenyl (ph), 1-naphthalene (1-nap), 2-naphthalene (2-nap), 9-anthracene (9-an), 1-pyrene (1-py), and 2-pyrene (2-py); M = W, Ar = ph, 2-nap] was synthesized and characterized. The photophysical properties of the complexes are reported, including short-lived emissive and long-lived nonemissive excited states, as well as the crystal and molecular structure of $Mo_2(O_2C-9\text{-an})_4$ together with electronic structure calculations employing density functional theory in order to aid the interpretation of some of the spectroscopic data. The work reported herein thus represents a new avenue in the photochemical studies of bimetallic quadruply bonded complexes.

Experimental Section

Materials. Benzoic acid, 2-naphthoic acid, 1-naphthoic acid, anthracene-9-carboxylic acid, and 1-pyrene carboxylic acid were purchased from commercial sources and used as received. $[Mo(CO)_6]$ was purchased from Strem and used as received. Ditungsten tetrapivalate,[16] $Mo_2(O_2C-ph)_4$ (**1**),[17] $W_2(O_2C-ph)_4$ (**5**),[18] $Mo_2(O_2C-1\text{-nap})_4$ (**2a**),[19] $Mo_2(O_2C-2\text{-nap})_4$ (**2b**),[19] $Mo_2(O_2C-9\text{-an})_4$ (**3**),[19] and pyrene-2-carboxylic acid[20] were prepared according to literature procedures.

$[Mo_2(O_2C-1\text{-py})_4]$ (4a). $Mo(CO)_6$ (0.59 g, 2.23 mmol) and pyrene-1-carboxylic acid (1.00 g, 4.06 mmol) were suspended in ca. 70 mL of 1,2-$C_6H_4Cl_2$/THF (4:1) and heated to 150 °C for 16 h. After allowing the reaction mixture to cool to room temperature, a red solid precipitated from the solution. This solid was isolated by filtration on a frit and washed with copious amounts of ethanol and then hexanes. Trace amounts of starting materials were removed by vacuum sublimation (ca. 10^{-3} Torr and ca. 100 °C) from the red solid (1.12 g, 85%). Microanalysis: found, C 69.98, H 3.65%. $C_{68}H_{36}Mo_2O_8$ requires C 69.63, H 3.09%. NMR (DMSO-d_6): δ_H (250 MHz) 8.28 (m, 7H), 9.04 (d, 1 H, J_{HH} = 8.2 Hz), 9.78 (d, 1 H, J_{HH} = 9.4 Hz). MALDI-MS: (1180.0981 100%, M^+).

$[Mo_2(O_2C-2\text{-py})_4]$ (4b). $Mo(CO)_6$ (0.59 g, 2.23 mmol) and pyrene-2-carboxylic acid (1.00 g, 4.06 mmol) were suspended in ca. 70 mL of 1,2-$C_6H_4Cl_2$/THF (4:1) and heated to 150 °C for 16 h. After allowing the reaction mixture to cool to room temperature, an orange crystalline solid precipitated from the solution. This solid was isolated by filtration on a frit and washed with copious amounts of ethanol and then hexanes. Trace amounts of starting materials were removed by vacuum sublimation (ca. 10^{-3} Torr and ca. 100 °C) from the orange solid (1.08 g, 82%). Microanalysis: found, C 69.73, H 3.46%. $C_{68}H_{36}Mo_2O_8$ requires C 69.63, H 3.09%. NMR (THF-d_8): δ_H (250 MHz) 7.28 (m, 4H), 7.50 (m, 5H). MALDI-MS: (1180.0981 100%, M^+).

$[W_2(O_2C-2\text{-nap})_4]$ (6). $[W_2(O_2C-^tBu)_4]$ (0.20 g, 0.26 mmol) and 2-naphthoic acid (0.25 g, 1.03 mmol) were dissolved in toluene (ca. 20 cm^3), resulting in the almost instant formation of a purple solution. The reaction was allowed to stir for 4 days during which time a purple solid formed. The purple solid (0.23 g, 87% yield) was collected by filtration and carefully washed with toluene and then hexanes. Microanalysis: found, C 49.91, H 2.31%. $C_{44}H_{28}W_2O_8$ requires C 50.22, H 2.68%. NMR (THF-d_8): δ_H (250 MHz) 7.42 (m, 2H), 7.86 (m, 3H), 8.36 (dd, 1 H, J_{HH} = 8.8 Hz), 8.56 (s, 1H). MALDI-MS: (1054.0837 100%, M^+).

Instrumentation. NMR spectra were recorded on either a 400 MHz Bruker DPX Avance-400 spectrometer or a 250 MHz Bruker DPX spectrometer. All ^1H NMR chemical shifts are reported in parts per million relative to the protio impurity in THF-d_8 at 3.58 ppm or DMSO-d_6 at 2.09 ppm. Microanalyses were carried out by Atlantic Microlab, Inc. Cyclic voltammetric and differential pulse voltammetric data were collected with the aid of a Princeton Applied Research (PAR) 173A potentiostat-galvanostat equipped with a PAR 176 current-to-voltage converter with *iR* compensation capability. A single-compartment voltammetric cell was equipped with a platinum working electrode, a platinum wire auxiliary electrode, and a pseudo-reference electrode consisting of a silver wire in 0.1 M $^nBu_4NPF_6$/THF separated from the bulk solution by a Vycor tip. Ferrocene was added as an internal reference. Decamethylferrocene was used as an internal reference when the oxidation potentials of complexes were close to that of ferrocene and the potentials were corrected later. Potentials were converted to the SCE scale using $E_{1/2}(FeCp_2^{+/0}) = +0.56$ V vs SCE. Single-crystal X-ray diffraction data were collected on a Nonius Kappa CCD diffractometer at 150 K using an Oxford Cryosystems Cryostream Cooler.

All photophysical measurements were carried out in 1 × 1 cm square quartz cuvettes equipped with Kontes stopcocks. Electronic absorption spectra at room temperature were recorded on a Hewlett-Packard diode array spectrometer (HP 8453), and the corrected steady-state luminescence spectra were recorded on a SPEX Fluoromax-2 spectrofluorimeter. Emission lifetime measurements and transient absorption spectra were measured on a home-built instrument pumped by a frequency doubled (532 nm) or tripled (355 nm) Spectra-Physics GCR-150 Nd:YAG laser (fwhm ~ 8 ns, ~5 mJ per pulse), and the signal from the photomultiplier tube (Hamamatsu R928) was processed by a Tektronics 400 MHz oscilloscope (TDS 380).[21,22] Lifetime decays were fitted using Sigma Plot 8.0.

Methods. All manipulations were performed in a nitrogen-filled glovebox or by using standard Schlenck line techniques in an atmosphere of oxygen-free UHP-grade argon. Solvents were dried over the appropriate drying agent and distilled prior to use. All solvents were stored in reservoirs equipped with Kontes taps over activated 4 Å molecular sieves, under an argon atmosphere and degassed prior to use.

Crystal data, details of data collection, data processing, structure analysis, and refinement are given in Table 1. The data collection strategy was set up to measure a quadrant of reciprocal space with a redundancy factor of 4, which means that 90% of the reflections were measured at 4. A combination of phi and omega scans with a frame width of 1.0° was used. Data integration was done with Denzo.[23] Scaling and merging of the data were done with Scalepack.[23] The structure was solved by the Patterson method with SHELXS-86.[24] There are two-half molecules in the asymmetric unit. Full-matrix least-squares refinements based on F^2 were performed in SHELXL-93.[25] The hydrogen atoms were included in the model at calculated positions using a riding model with U(H) = 1.2* Ueq(bonded C atom). Neutral atom scattering factors were used and include terms for anomalous dispersion.

(12) Miskowski, V. M.; Goldbeck, R. A.; Kliger, D. S.; Gray, H. B. *Inorg. Chem.* **1979**, *18*, 86.
(13) Hopkins, M. D.; Gray, H. B. *J. Am. Chem. Soc.* **1984**, *106*, 2468.
(14) Hsu, T.-L. C.; Engebretson, D. S.; Helvoigt, S. A.; Nocera, D. G. *Inorg. Chim. Acta* **1995**, *240*, 551.
(15) Chang, I. J.; Nocera, D. G. *Inorg. Chem.* **1989**, *28*, 4309.
(16) Santure, D. J.; Huffman, J. C.; Sattelberger, A. P. *Inorg. Chem.* **1985**, *24*, 371.
(17) McCarley, R. E.; Templeton, J. L.; Colburn, T. J.; Katovic, V.; Hoxmeier, R. J. *Adv. Chem. Ser.* **1976**, *150*, 318.
(18) Cotton, F. A.; Wang, W. *Inorg. Chem.* **1984**, *23*, 1604.
(19) Hochberg, E.; Walfs, P.; Abbott, E. H. *Inorg. Chem.* **1974**, *13*, 1824.
(20) Barfield, M.; Collins, M. J.; Gready, J. E.; Sternhell, S.; Tansey, C. W. *J. Am. Chem. Soc.* **1989**, *111*, 4285.
(21) Bradley, P. M.; Bursten, B. E.; Turro, C. *Inorg. Chem.* **2001**, *40*, 1376.
(22) Warren, J. T.; Chen, W.; Johnston, D. H.; Turro, C. *Inorg. Chem.* **1999**, *38*, 6187.
(23) Otwinowski, Z.; Minor W. *Macromolecular Crystallography*, Part A; Academic Press: New York, 1997.
(24) Sheldrick, G. M. *Acta Crystallog., Sect. A* **1990**, *46*, 467.
(25) Sheldrick, G. M. *SHELXL-93*; Universität Göttingen: Göttingen, Germany, 1993.

Table 1. Summary of Crystallographic Data for $[Mo_2(O_2C\text{-}9\text{-an})_4]\bullet(C_4H_8O)_2$ (**3**)

Formula	$C_{68}H_{52}O_{10}Mo_2$
FW (g mol-1)	1,220.98
Crystal System	Monoclinic
Color	Orange
Crystal size (mm)	$0.04 \times 0.25 \times 0.35$
Space Group	$P21/c$
Temperature (K)	150(2)
a (Å)	22.784(2)
b (Å)	22.806(2)
c (Å)	10.395(1)
β (°)	95.20(1)
Volume (Å^3)	5,379.3(8)
Z	4
Density$_{calc}$ (g/cm^3)	1.508
Wavelength (Å)	0.71073
Abs Coeff (mm^{-1})	0.531
Theta range (°)	2.16−27.46
Reflections collected	88,960
Independent reflections (Rint)	12,319 (0.046)
R1(F) [I > 2σ(I)]	0.0319
R1(F) (all data)	0.0521
WR2(F2) (all data)	0.0802
Goodness of Fit	1.015

Molecular and electronic structure determinations on $[Mo_2(O_2C-9\text{-an})_4]$ were performed with density functional theory (DFT) using the Gaussian 98[26] package employing the B3LYP[27−29] functional in conjunction with the 6-31G* (SD) basis set for H, C, and O,[30] and the SDD energy consistent pseudopotentials for Mo.[31] All geometries were fully optimized at the above levels using the default optimization criteria of the program. Orbital analyses were completed with GaussView.[32]

Results and Discussion

Synthesis and Characterization. The structures and numbering scheme of the $Mo_2(O_2C-R)_4$ complexes are shown in Figure 1. The extension of the π-electronic system of aromatic rings was tuned across the series, and two of these complexes, **1** and **2b**, were compared to their tungsten analogues, **5** and **6**, respectively. The positions of the carboxylate group on the aromatic rings were also adjusted in order to study the effect of the degree of conjugation between the aromatic ring and the carboxylate on the photophysical properties of the molecules.

The molybdenum complexes were prepared from reactions between slightly less than 2 equiv of the corresponding free arylcarboxylic acid and $Mo(CO)_6$ in a refluxing mixture of 1,2-$C_6H_4Cl_2$/THF for 16 h. The tungsten complexes were prepared by either a sodium reduction of WCl_4 in the presence of the sodium benzoate or a metathetic route involving 4 equiv of the free arylcarboxylic acid and $[W_2(O_2C\text{-}^t\text{Bu})_4]$ in THF. The preparation of the benzoate complexes was previously reported, and they were prepared with great care being taken to ensure their purity.[10]

The molybdenum compounds were washed with ethanol followed by hexanes, and any remaining starting materials were subsequently sublimed off. The complexes all colored and range from yellow to purple. The compounds are air- and moisture-sensitive, with the tungsten compounds being more reactive in this respect. All preparations and manipulations were therefore carried out under purified atmospheres of nitrogen and argon with the use of dry and deoxygenated solvents.

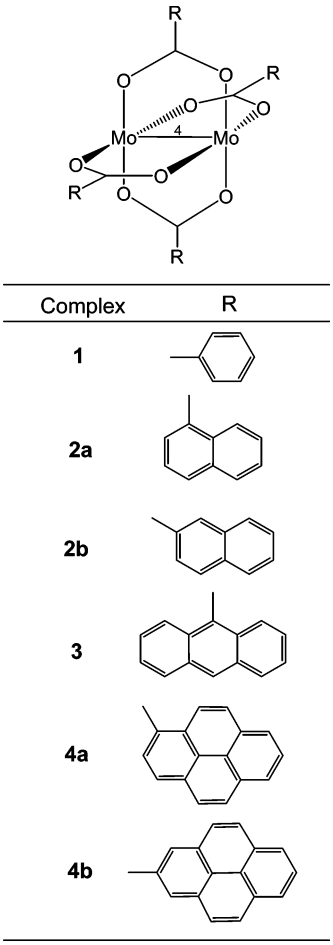

Figure 1. Schematic representation of the molecular structures of the quadruply bonded dimolybdenum complexes. Complexes **5** and **6** are the tungsten analogues of **1** and **2b**, respectively.

Several compounds of formula $M_2(O_2C-Ar)_4$ have been previously crystallographically characterized, including $W_2(O_2C-ph)_4$ and $W_2(O_2C-2,4,6\text{-}Me_3-C_6H_2)_4$.[18] The introduction of the 2,6-methyl groups onto the aromatic ring was shown by Cotton et al. to cause the blades of the phenyl rings to be severely twisted with respect to the O_2C planes, whereas in the benzoate, relatively small O_2C-C_6 dihedral angles were observed, thus allowing for conjugation of the C_6 and O_2C π-systems.[33−35] For this reason and for others described later, we have determined the molecular structure of $Mo_2(O_2C-9\text{-an})_4$ (9-an = 9-anthracene) in the solid state. We also carried out electronic structure calculations on this compound by employing density functional theory to aid in interpreting the bonding and spectroscopy.

Solid-State Structure. An ORTEP drawing of $[Mo_2(O_2C\text{-}9\text{-an})_4]\bullet(C_4H_8O)_2$ is shown in Figure 2, and the pertinent metrical data are given in Table 2. A complete list of the bond lengths

(26) Frisch, M. J. et al. *Gaussian 98*; Gaussian, Inc.: Pittsburgh, PA, 1998.
(27) Becke, A. D. *J. Chem. Phys.* **1993**, *98*, 5648.
(28) Becke, A. D. *Phys. Rev. A: At. Mol. Opt. Phys.* **1998**, *38*, 3098.
(29) Lee, C.; Yang, W.; Parr, R. G. *Phys. Rev. B: Condens. Matter Mater. Phys.* **1988**, *37*, 785.
(30) Hehre, W. J.; Radom, L.; Schleyer, P. v. R.; Pople, J. A. *Ab initio Molecular Orbital Theory*; John Wiley & Sons: New York, 1986.
(31) Andrae, D.; Haeussermann, U.; Dolg, M.; Stoll, H.; Preuss, H. *Theor. Chim. Acta* **1990**, *77*, 123.
(32) *Gaussian 88*; Gaussian Inc.: Pittsburgh, PA, 1988.
(33) San Filippo, J., Jr.; Sniadoch, H. J. *Inorg. Chem.* **1976**, *15*, 2209.
(34) Chisholm, M. H.; Huffman, J. C.; Iyer, S. S.; Lynn, M. A. *Inorg. Chim. Acta* **1996**, *243*, 283.
(35) Chisholm, M. H.; Clark, D. L.; Huffman, J. C.; Van der Sluys, W. G.; Kober, E. M.; Lichtenberger, D. L.; Bursten, B. E. *J. Am. Chem. Soc.* **1987**, *109*, 6796.

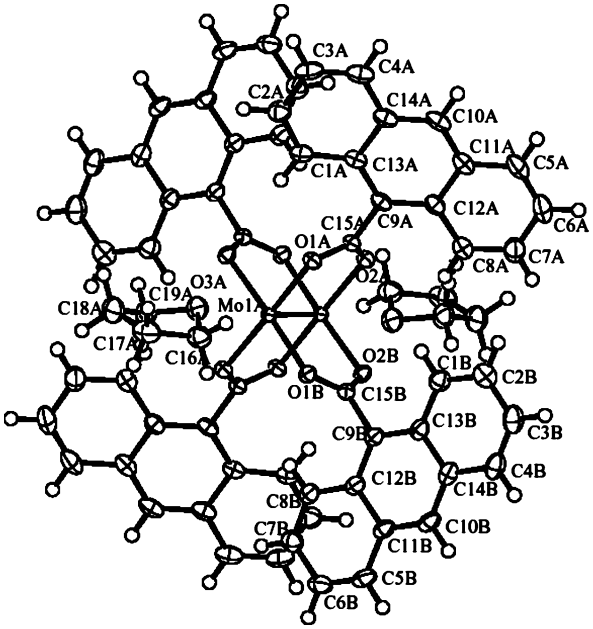

Figure 2. ORTEP view of one of the molecules in the asymmetric unit of $Mo_2(O_2C-9\text{-an})_4$ (**3**). Hydrogen atoms have been omitted for clarity.

and angles is given in the Supporting Information. The dimolybdenum unit lies on an inversion center, and the asymmetric unit cell consists of two crystallographically independent halves of the molecule. The Mo−Mo bond distances (ca. 2.104 Å) fall within the expected range for dimolybdenum tetracarboxylate complexes,[10] and similarly, the Mo−O distances span a narrow, but again expected range (2.102(2)−2.135(2) Å), as shown in Table 2. All of the carboxylate groups are bonded in a regular fashion, imparting approximate D_{4h} symmetry to the Mo_2O_8 core of the molecule. Perhaps the most interesting feature of this compound is the arrangement of the anthracenyl groups about the Mo_2O_8 core. The dihedral angles defined by the planes composed of the carbon atoms of the anthracene and the dimolybdenum atoms with the carboxylate atoms are ca. 45° (oblique) and ca. 85° (perpendicular) (see Table 3). Steric hindrance between the anthracenyl *peri*-H atoms in the 1- and 8-positions with the carboxylate O atoms presumably prevents carboxylate groups from being coplanar with the anthracene unit. Similar dihedral angles of 85.2(1) and 86.3(1)° were found between the planes defined by the phenyl rings and the carboxylate atoms for all four mesityl carboxylates in $[W_2(O_2C-2,4,6\text{-}Me_3-C_6H_2)_4]$.[18] Smaller dihedral angles were found between the phenyl rings and the carboxylate atoms of 9.9(1) and 12.5(1)° for $[W_2(O_2C-C_6H_5)_4]$.[18] A twist angle between the carboxylic group and the anthracene of ca. 55 and ca. 45° was calculated for anthracene-9-carboxylic acid in the ground and excited states, respectively, using semiempirical AM1 calculations, and is consistent with that found in the crystal structure of anthracene-9-carboxylic acid.[36] Kitagawa et al. have also recently reported on similar dihedral angles between the anthracene moieties and the carboxylate plane in $Ru(O_2C-9\text{-an})_4(THF)_2$, with the perpendicular dihedral angles attributed to π-stacking interactions in the crystal.[37]

Bonding and Electronic Considerations. Given the relatively low symmetry (C_i) of both crystallographically independent molecules of $[Mo_2(O_2C\text{-}9\text{-an})_4]\bullet 2C_4H_8O$, electronic structure calculations were carried out using density functional theory (DFT) with the Gaussian 98[26] package employing the B3LYP[27−29] functional in conjunction with the 6-31G* (5D) basis set for H, C, and O,[30] and the SDD energy consistent pseudopotentials for Mo.[31] The utility of such DFT calculations has previously been demonstrated for calculating the bonding and electronic structures of the "dimer of dimer" complexes $[\{M_2(O_2C\text{-}^tBu)_3\}_2(\mu\text{-}O_2CCO_2)]$ (M = Mo, W) and $[\{M_2(O_2C\text{-}^tBu)_3\}_2(\mu\text{-}O_2C\text{-}X\text{-}CO_2)]$ (M = Mo, W; X = 1,4-C_6F_4, 9,10-$C_{14}H_8$).[38,39]

Table 2. Selected Metrical Data for the Two Crystallographically Independent Molecules of $[Mo_2(O_2C\text{-}9\text{-an})_4]\bullet(C_4H_8O)_2$ (**3**)[a]

Bond Lengths	Å
Mo(1A)-Mo(1A) #1	2.1041(3)
Mo(1A) − O(2A) #1	2.102(2)
Mo(1A) − O(1A)	2.106(2)
Mo(1A) − O(1B)	2.1075(14)
Mo(1A) − O(2B) #1	2.1209(14)
Mo(1B)-Mo(1B) #2	2.1049(4)
Mo(1B) − O(1C)	2.108(2)
Mo(1B) − O(1D)	2.1079(2)
Mo(1B) − O(2C) #2	2.112(2)
Mo(1B) − O(2D) #2	2.135(2)
Mo(1A) − O(3A) (THF)	2.573(2)
Mo(1B) − O(3B) (THF)	2.563(2)
Bond Angles	**Degrees**
O(2A)#1 − Mo(1A) − Mo(1A)#1	91.26(4)
O(2A)#1 − Mo(1A) − O(1A)	176.67(6)
Mo(1A)#1 − Mo(1A) − O(1A)	91.93 (4)
O(2A)#1 − Mo(1A) − O(1B)	88.29(6)
Mo(1A)#1 − Mo(1A) − O(1B)	93.07(4)
O(1A) − Mo(1A) − O(1B)	90.58(6)
O(2A)#1 − Mo(1A) − O(2B)#1	91.30(6)
Mo(1A)#1 − Mo(1A) − O(2B) #1	90.40(4)
O(1A) − Mo(1A) − O(2B) #1	89.63(6)
O(1B) − Mo(1A) − O(2B)#1	176.52(5)
C(15A) − O(1A) − Mo(1A)	117.28(14)
C(15A) − O(2A) − Mo(1A)#1	118.01(13)
C(15B) − O(1B) − Mo(1A)	116.06(13)
O(1C) − Mo(1B) − Mo(1B)#2	90.99(4)
Mo(1B)#2 − Mo(1B) − O(1D)	92.42(4)
O(1C) − Mo(1B) − O(2D)	88.39(6)
Mo(1B)#2 − Mo(1B) − O(2C)#2	92.27(4)
O(1C) − Mo(1B) − O(2C)#2	176.61(6)
O(1D) − Mo(1B) − O(2C)#2	90.54(2)
Mo(1B)#2 − Mo(1B) − O(2D)#2	90.88(4)
O(1C) − Mo(1B) − O(2D)#2	91.16(6)
O(1D) − Mo(1B) − O(2D)#2	176.68(6)
O(2C)#2 − Mo(1B) − O(2D)#2	89.72(6)
C(15C) − O(1C) − Mo(1B)	118.44(14)
C(15C) − O(2C) − Mo(1B)#2	116.87(13)
C(15D) − O(1D) − Mo(1B)	117.11(14)
C(15D) − O(2D) − Mo(1B)#2	117.34(14)

[a] Symmetry transformations used to generate equivalent atoms: #1) -x, -y, -z+1 and #2) −x+1, -y+1, -z+1.

Table 3. Selected Dihedral Angles for Both Crystallographically Independent Molecules of $[Mo_2(O_2C\text{-}9\text{-an})_4]\bullet(C_4H_8O)_2$ (3)

Plane 1	Plane 2	Dihedral angles (deg)
C(1A) to C(14A)	Mo(1A)/Mo(1A)#1/O(1A)/O(2A)/C(15A)	47.30(6)
C(1B) to C(14B)	Mo(1A)/Mo(1A)#1/O(1B)/O(2B)/C(15B)	82.18(5)
C(1C) to C(14C)	Mo(1B)/Mo(1B)#1/O(1C)/O(2C)/C(15C)	44.30(5)
C(1D) to C(14D)	Mo(1B)/Mo(1B)#1/O(1D)/O(2D)/C(15D)	87.81(6)

(36) Fitzgerald, L. J.; Gerkin, R. E. *Acta Crystallogr.* **1997**, *C53*, 71.
(37) Furukawa, S.; Kitagawa, S. *Inorg. Chem.* **2004**, *43*, 6464.
(38) Bursten, B. E.; Chisholm, M. H.; Clark, R. J. H.; Firth, S.; Hadad, C. M.; Wilson, P. J.; Woodward, P. M.; Zaleski, J. M. *J. Am. Chem. Soc.* **2002**, *124*, 12244.

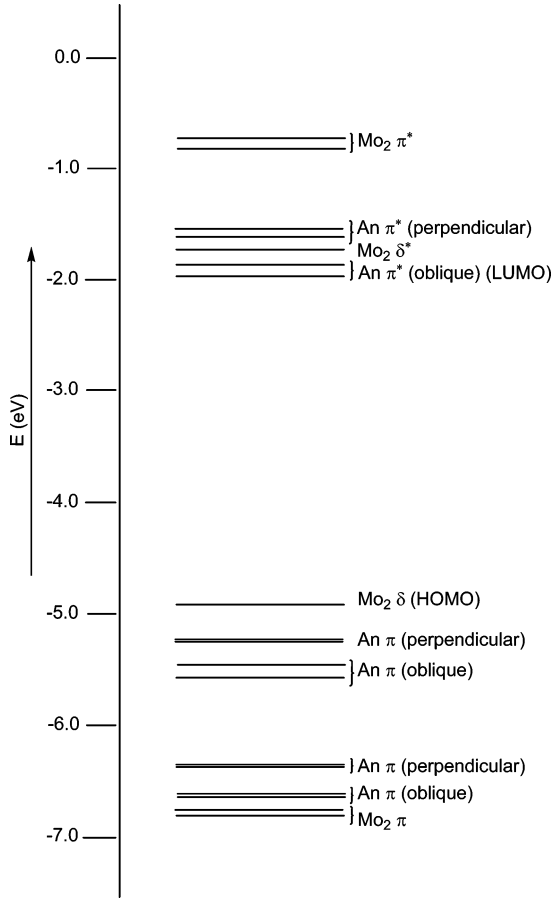

Figure 3. Frontier molecular orbital energy diagram of $Mo_2(O_2C-9\text{-an})_4$ (**3**).

By using the coordinates of one molecule found in the unit cell of $[Mo_2(O_2C\text{-}9\text{-an})_4]\bullet 2C_4H_8O$ (neglecting the axially coordinated THF molecules), a single-point calculation was undertaken using the default criterion. A molecular orbital (MO) energy level diagram for the frontier molecular orbitals is given in Figure 3, and the calculated frontier molecular orbitals are shown in Figure 4. The HOMO is clearly Mo_2 δ based with some π character from the anthracene that is twisted ca. 45° to the carboxylate atoms. The next eight occupied molecular orbitals may be divided into two groups of four, in which the molecular orbitals of the first group lie within 0.3 eV in energy of each other and are less than 1 eV lower than that of the HOMO, and the second group are up to another 1 eV lower in energy and are separated from each other by 0.2 eV. The HOMO-1 and HOMO-2 are the π orbitals of the anthracenyl units that are perpendicular to their respective carboxylate groups and are related to each other by an inversion center with gerade (g) and ungerade (u) symmetry, respectively. The HOMO-3 and HOMO-4 are based on the anthracenyl groups that are oblique with respect to the carboxylate group and have u and g symmetry, respectively. HOMO-5 and HOMO-6 are based entirely on the perpendicular anthracenyl units and have u and g symmetry, respectively. HOMO-7 and HOMO-8 are the π-based orbitals of the oblique anthracenyl groups. HOMO-9 and HOMO-10 are the Mo_2 π-based orbitals. The LUMO and LUMO+1 are the oblique anthracenyl π^* orbitals, and the latter appears to have a small Mo_2 δ contribution. The next orbital higher in energy, the LUMO+2, is clearly Mo_2 δ^* based and is antibonding with respect to all four carboxylates. The LUMO+3 and LUMO+4 are the perpendicular anthracenyl π^* orbitals with the former also having a small Mo_2 δ^* contribution. LUMO+5 and LUMO+6 are Mo_2 π^* based.

A full optimization of the above structure in C_i symmetry resulted in a structural rearrangement of the anthracenyl groups. Dihedral angles between the anthracenes and the carboxylate atoms in the optimized structure were found to be ca. 35 and 50°. Clearly, in the solid-state structure, intermolecular packing forces are likely to play a significant role. As the O_2C-anthracene dihedral angles change, so do the relative energies of the nearly degenerate π and π^* orbitals labeled in Figure 3 as oblique and perpendicular. As the energies involved in changing these angles are relatively small, it is expected that the effect that this rotation will have on the absorption spectrum of the molecule in solution is to broaden the $Mo_2(\delta) \rightarrow L(\pi^*)$ transitions.

On the basis of these calculations, we can consider a similar ordering of frontier MOs for the other $Mo_2(O_2C-Ar)_4$ compounds and, furthermore, that the tungsten complexes will have a M_2 manifold of bonding MOs that are roughly 0.5 eV higher in energy than those of their molybdenum analogues.

Electrochemistry. The electrochemical oxidation and reduction potentials of complexes **1**−**6** in THF (298 K) are listed in Table 4. For the Mo_2 complexes, with the exception of complex **3**, the oxidation potential is relatively insensitive to the aryl substituent of the carboxylate ligands and is observed in the 0.50−0.57 V vs SCE range (Table 4). As previously reported, the oxidation from the HOMO Mo−Mo δ orbital is slightly more difficult for $Mo_2(O_2C-R)_4$ complexes, where R = aryl than R = alkyl ($E_{1/2} \sim 0.49$ V vs SCE).[34,40] In addition, it has also been shown that the stability of the δ orbital increases with the electron-withdrawing ability of the substituent R′ in $Mo_2(O_2C\text{-}p\text{-}R'\text{-}C_6H_4)_4$, thus making it more difficult to remove an electron from the bimetallic core for R′ = NO_2 than R′ = OCH_3.[34,40] Complex **3** is more difficult to oxidize than the other Mo_2 carboxyaryl systems listed in Table 4 by ~0.2 V. The crystal structure shows that the anthracene part of each ligand in **3** is twisted with respect to the Mo_2O_2C plane, thus decreasing the conjugation between the O_2C unit and the anthracene. Owing to steric hindrance, this dihedral twist is expected to persist in solution, as is also predicted by the structural optimization. A similar increase in oxidation potential was reported for $Mo_2(O_2C-2,6\text{-}Me_2-C_6H_3)_4$, a complex in which the 2,6-$Me_2-C_6H_3$ unit is twisted with respect to the O_2C plane, relative to the conjugated $Mo_2(O_2C-3,5\text{-}Me_2-C_6H_3)_4$.[40] As reported previously, the W_2 complex **5** is significantly easier to oxidize than the corresponding Mo_2 complex **1**.[34]

Reversible reduction waves are observed for complexes **1**−**6**, with potentials dependent on the aryl substituents (Table 4). It is readily apparent from Table 4 that, for the Mo_2 series (**1**−**4**), the complexes are easier to reduce as the π-system of the aryl substituent is extended (with the exception of **4b**). This variation in reduction potential with substituent is indicative of a ligand π^* LUMO centered on the aromatic portion of the carboxyaryl ligands. The reduction potential of **5** is slightly more negative

(39) Byrnes, M. J.; Chisholm, M. H.; Dye, D. F.; Hadad, C. M.; Pate, B. D.; Wilson, P. J.; Zaleski, J. M. *Dalton Trans.* **2004**, 523.

(40) Chisholm, M. H.; Glasgow, K. C.; Klein, L. J.; Macintosh, A. M.; Peters, D. C. *Inorg. Chem.* **2000**, *39*, 4354.

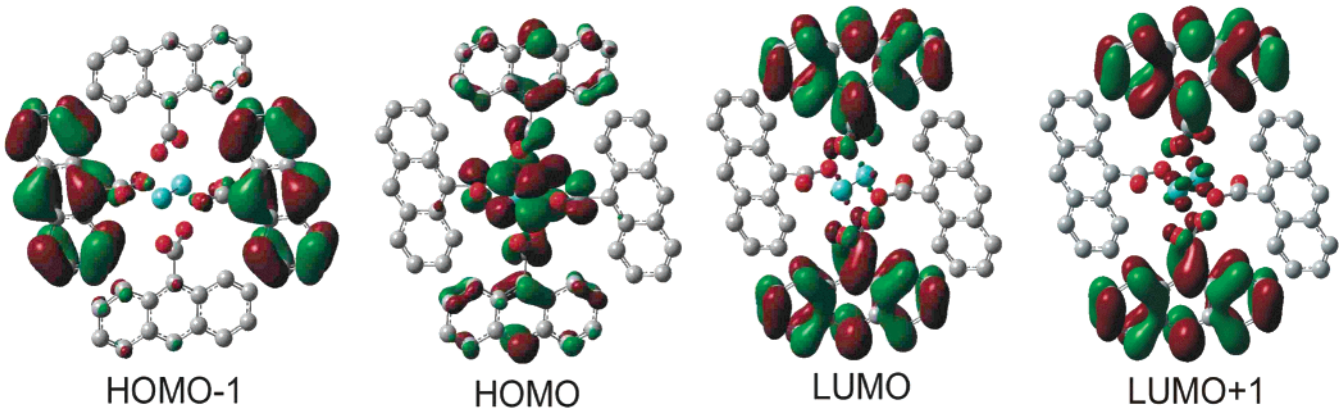

Figure 4. GaussView representations of the frontier molecular orbitals of $Mo_2(O_2C-9\text{-an})_4$ (**3**).

Table 4. Absorption (λ_{abs}) Maxima and Redox Potentials of the Complexes in THF

Complex	λ_{abs}/nm(ϵ/× 10^3 $M^{-1}cm^{-1}$)	$E_{1/2}^{ox}$/V[a]	$E_{1/2}^{red}$/V[a]
1	425 (36.9)	0.51[b]	−2.26[c]
2a	277 (25.7), 317(9.5), 461(27.9)	0.50[b]	−1.97[c]
2b	295 (22.3), 464 (15.3)	0.55[b]	−1.96[c]
3	332 (16.7), 347(23.8), 365 (32.2), 385 (31.0), 460(10.9)	0.75[b]	−1.70[c]
4a	353 (18.9), 517 (6.6)	0.55[b]	−1.58[c]
4b	308 (37.8), 322(77.0), 337 (69.0), 465 (40.5)	0.57[b]	−1.90, −2.1
5	552 (32.2), 592 (33.1)	0.03[b]	−2.36[c]
6	598 (40.2), 645 (45.4)	−0.06[b]	−1.86[c]

[a] vs SCE, 0.1 M nBu$_4$NPF$_6$. [b] One-electron process. [c] Two-electron process.

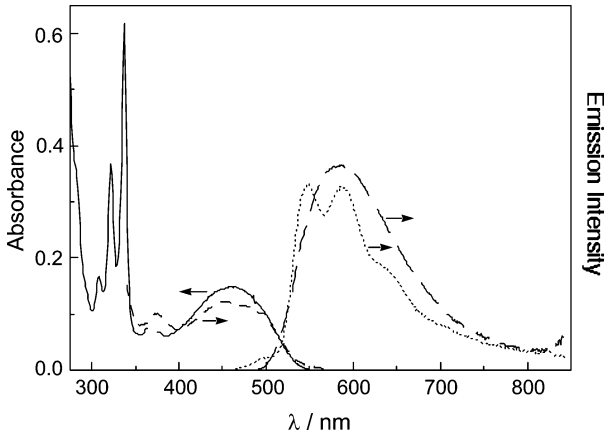

Figure 5. Electronic absorption (—), emission (– – –, λ_{exc} = 465 nm), and excitation (- - -, λ_{em} = 585 nm) of **4b** in THF at 298 and 77 K luminescence of **4b** in 2-Me-THF (· · ·, λ_{exc} = 465 nm).

than that of **1**, also consistent with a ligand-based reduction. These results are consistent with the electronic structure calculations presented in Figures 3 and 4, which predict a metal-centered HOMO and a ligand π^* LUMO.

Electronic Absorption. The absorption maxima and intensities of complexes **1**−**6** are listed in Table 4 at room temperature in THF, and a typical spectrum collected for **4b** is shown in Figure 5. The absorption bands with vibronic structure observed between 270 and 400 nm for complexes **2**−**4** and **6** are assigned to ligand-centered (LC) $^1\pi\pi^*$ transitions associated with each corresponding aryl−carboxylate ligand. The electronic absorption spectra of the free aryl carboxylic acids in THF confirm this assignment.

The $^1\delta\delta^*$ transition in $Mo_2(O_2C-R)_4$ (R = H, alkyl, aryl) complexes is weak and is typically observed at ∼436 nm ($\epsilon \sim$ 100 M^{-1} cm^{-1}).[10,41,42] The broad absorption observed in the 400−600 nm region for the Mo_2 complexes in Table 4 exhibits molar extinction coefficients of $\sim 10^4$ M^{-1} cm^{-1}. In the related $Mo_2(O_2C-R)_4$ (R = C_6H_5, substituted phenyl), intense transitions in the visible region ($\epsilon \sim 10^4$ M^{-1} cm^{-1}) have previously been assigned as spin-allowed metal-to-ligand charge transfer (^{1}MLCT) arising from Mo_2 $\delta \rightarrow O_2C$ π^*.[16,33,40,42−44] The red-shift in the lowest energy transition along the series **1**, **2a** and **2b**, and **4a** is consistent with this assignment (Table 4); these complexes possess similar oxidation potentials, with the electron being removed from their Mo_2 δ HOMO, and reduction potentials that parallel the energy of the aryl π^* LUMO. Although the anthracene ring in **3** is easier to reduce than the benzene, 1-naphthalene, and 2-naphthalene rings in **1**, **2a**, and **2b**, respectively, the measured oxidation potential of **3** indicates a greater stabilization of the δ HOMO, thus shifting the Mo_2 $\delta \rightarrow O_2C$ π^* ^{1}MLCT transition to an energy similar to those observed for **2a** and **2b**. Similarly, the reduction potential of **4b** is similar to those of **2a** and **2b**, again placing the ^{1}MLCT transition of the 2-pyrene complex at a similar energy to those of the naphthalene derivatives. As expected, the $W_2(O_2C-R)_4$ complexes **5** (R = ph) and **6** (R = 2-nap) exhibit red-shifted ^{1}MLCT transitions relative to the corresponding dimolybdenum systems owing to the ease of oxidation of the ditungsten core (Table 4).

The maximum of the lowest energy transition of **1** shifts from 425 to 443 nm at room temperature from THF to DMSO as solvents. Similarly, a shift was observed changing the solvent from THF to DMSO from 464 to 480 nm and from 517 to 527 nm for **2b** and **4a**, respectively. These shifts are also consistent with a charge-transfer transition since the position of absorption peaks assigned as arising from $^1\delta\delta^*$ transitions are relatively independent of solvent.[12,45]

Steady-State Luminescence. Complexes **1**−**6** exhibit weak emission at room temperature in THF with emission quantum yields, Φ_{em}, estimated to be $\sim 10^{-5}$ and maxima listed in Table

(41) Chisholm, M. H. *J. Organomet. Chem.* **2002**, *641*, 15.
(42) Norman, J. G. J.; Kolari, H. J.; Gray, H. B.; Trogler, W. C. *Inorg. Chem.* **1977**, *16*, 987.
(43) Cotton, F. A.; Donahue, J. P.; Murillo, C. A.; Perez, L. M.; Yu, R. M. *J. Am. Chem. Soc.* **2003**, *125*, 8900.
(44) Cotton, F. A.; Donahue, J. P.; Murillo, C. A.; Perez, L. M. *J. Am. Chem. Soc.* **2003**, *125*, 5486.
(45) Cotton, F. A.; Curtis, N. F.; Johnson, B. F. G.; Robinson, W. R. *Inorg. Chem.* **1965**, *4*, 326.

Table 5. Photophysical Data for Complexes **1** − **6**

Complex	λ_{em}/nm[a]	λ_{em}/nm[b]	E_{00}/eV[c]	ΔE/cm^{-1} [f]	τ_{ta}/μs
1	562	521	2.38	5,736	58
2a	650	587	2.11	6,307	50
2b	602	558	2.22	4,940	43
3	743	630	1.97	8,280	76
4a	707	*d*	2.10[e]	5,198	69
4b	585	548	2.26	4,411	74
5	645	639	1.94	1,388	0.058
6	711	*d*	1.96[e]	1,439	0.075

[a] In THF at 298K. [b] Position of highest energy vibronic emission peak in a 2-Me-THF glass at 77K. [c] From 77K emission unless otherwise noted. [d] Not soluble in 2-MeTHF. [e] Estimated from the onset of the emission at 298K. [f] Stokes shift at 298K.

5. For all complexes, the emission bands are broad and nearly structureless in solution at room temperature. Typical emission and excitation spectra are shown in Figure 5 for **4b**. The excitation spectra collected at the emission maximum are in good agreement with the absorption spectrum of each complex, indicative of a single low-energy emissive state. Room temperature $^1\pi\pi^*$ fluorescence and $^3\pi\pi^*$ low temperature (77 K) phosphorescence spectra of the free aromatic carboxylic acid ligands reveal that the emission observed for complexes **1**−**6** does not originate from $\pi\pi^*$ states of the ligands. Along with the excitation spectra, this observation also rules out the possibility that the luminescence arises from a small amount of free ligand impurity.

In general, the Stokes shifts observed at room temperature for the series of Mo_2 complexes were in the range of 4411 to 6307 cm^{-1}, with the exception of complex **3**, for which the Stokes shift was measured to be 8280 cm^{-1} (Table 5). The magnitude of these Stokes shifts, ΔE, is greater than those previously reported for the fluorescence from the metal-centered (MC) $^1\delta\delta^*$ excited states of quadruply bonded complexes, such as $Mo_2Cl_4(PBu_3)_4$, $[Mo_2Cl_8]^{4-}$, and $W_2Cl_4(dppm)_2$ (dppm = bis-(diphenylphosphino)methane), which range from 2000 to 3000 cm^{-1}.[12,46,47] The phosphorescence from the $^3\delta\delta^*$ excited state of quadruply bonded dirhenium(III,III) complexes was recently reported to exhibit an energy difference between the absorption and emission of ~13 000 cm^{-1}, however, the luminescence from both the $^1\delta\delta^*$ and $^3\delta\delta^*$ excited states is independent of solvent. In contrast, the emission from the complexes reported here depends on solvent polarity. For example, for complexes **1**, **2b**, and **4a**, a shift in the emission maxima from 562, 602, and 707 nm in THF to 605, 658, and 748 nm in DMSO is observed, respectively. Such solvent dependence is typical of luminescence from a charge-transfer state.[48−50]

The emission maxima of the highest energy vibronic component of each complex collected at 77 K in a 2-Me-THF glass are listed in Table 5, and the low-temperature emission spectrum of **4b** is shown in Figure 5. The origin of the 77 K emission was used to calculate the excited-state energy of the emissive state of each complex, E_{00} (Table 5). For all of the complexes, a vibronic progression with $\Delta\nu$ that ranges from 1000 to 1400 cm^{-1} is observed in the emission spectra at 77 K. Vibronic progressions previously reported for the luminescence of quadruply bonded $^1\delta\delta^*$ and $^3\delta\delta^*$ excited states typically correspond to the metal−metal stretching frequency and are in the 200 to 350 cm^{-1} range.[10,12,13,47] The observed Stokes shift, solvent dependence, and vibronic progression rule out the emission from complexes **1**−**4** as arising from the $^1\delta\delta^*$ or $^3\delta\delta^*$ excited states.

As shown in Figure 5 for complex **4b**, the emission spectrum obtained at 77 K in a 2-methyl-THF glass is blue-shifted with respect to that collected in THF at 298 K. Thermally induced Stokes shifts from 77 to 298 K of 0.14 to 0.20 eV were observed for **1**, **2a**, **2b**, and **4b**, which are typical of MLCT luminescence in mononuclear complexes.[48] In addition, the observed vibronic progressions are consistent with vibrations of the aromatic carboxylic acid ligands and are also observed in low-temperature luminescence spectra from MLCT excited states of complexes which possess aromatic ligands, such as $[Ru(bpy)_3]^{2+}$.[51,52]

The excited-state energy, E_{00}, of the emissive state listed in Table 5 correlates well with the HOMO−LUMO gaps calculated for each complex from the corresponding ground-state oxidation and reduction potentials (Table 4). Such correlation between the redox potentials and E_{00} is well-established for Ru(II) complexes that exhibit MLCT emission.[53] From the Stokes shift, solvent dependence, the vibronic progression in the luminescence observed at 77 K, and the correlation of E_{00} with the HOMO−LUMO gap, it may be concluded that the luminescence in these complexes arises from an MLCT state with electron configuration (Mo_2 δ)^1(O_2C−aryl π^*)^1. It should be noted that the emission of **3** exhibits a greater Stokes shift at room temperature and a larger thermally induced blue shift than the other dimolybdenum complexes from 77 to 298 K. These shifts are consistent with a greater nuclear displacement of the emissive state with respect to the ground state in **3** compared to the other complexes. Population of the unoccupied π^* orbital of aryl carboxylates is known to result in greater conjugation between the O_2C and aryl components, thus increasing the planarity between the two units.[54−63] Therefore, in an MLCT excited state resulting from a $Mo_2(\delta) \rightarrow O_2C$−aryl($\pi^*$) transition, an increase in planarity of the carboxylate ligand is expected owing to the increased electron density in the ligand's π^* orbital. The crystal structures of **1**[64] and **5**[18] show that, in the ground state, the O_2C and aryl components of the carboxylate ligands are nearly coplanar, whereas in **3**, steric hindrance results in a dihedral angle of ~54° between the two units. From these considerations, it may be hypothesized that there is a greater nuclear displacement between the equilibrium positions of the ground state and MLCT excited state of **3** compared to the other

(46) Fleming, R. H.; Geoffroy, G. L.; Gray, H. B.; Gupta, A.; Hammond, G. S.; Kliger, D. S.; Miskowski, V. M. *J. Am. Chem. Soc.* **1976**, *98*, 48.
(47) Macintosh, A. M.; Nocera, D. G. *Inorg. Chem.* **1996**, *35*, 7134.
(48) Chen, P. Y.; Meyer, T. J. *Chem. Rev.* **1998**, *98*, 1439.
(49) Kober, E. M.; Sullivan, B. P.; Meyer, T. J. *Inorg. Chem.* **1984**, *23*, 2098.
(50) Wasielewski, M. R.; Minsek, D. W.; Niemczyk, M. P.; Svec, W. A.; Yang, N. C. *J. Am. Chem. Soc.* **1990**, *112*, 2823.
(51) Van der Burgt, M. J.; Huizer, A. H.; Varma, C. A. G. O.; Wagner, B. D.; Lusztyk, J. *Chem. Phys.* **1995**, 193.
(52) Neugebauer, J.; Baerends, E. J.; Efremov, E. V.; Ariese, F.; Gooijer, C. *J. Phys. Chem. A* **2005**, *109*, 2100.
(53) Vlcek, A. A.; Dodsworth, E. S.; Pietro, W. J.; Lever, A. B. P. *Inorg. Chem.* **1995**, *34*, 1906.
(54) Werner, T. C.; Hercules, D. M. *J. Phys. Chem.* **1969**, *73*, 2005.
(55) Werner, T. C.; Matthews, T.; Soller, B. *J. Phys. Chem.* **1976**, *80*, 533.
(56) Weller, A.; Urban, W. *Angew. Chem.* **1954**, *66*, 336.
(57) Becker, H.-D. *Chem. Rev.* **1993**, *93*, 145.
(58) Plummer, B. F.; Hamon, S.; Burke, J. A. I. *J. Phys. Chem.* **1987**, *91*, 2022.
(59) Swayambunathan, V.; Lim, E. C. *J. Phys. Chem.* **1987**, *91*, 6359.
(60) Berberan-Santos, M. N.; Prieto, M. J. E.; Szabo, A. G. *J. Phys. Chem.* **1991**, *95*, 5471.
(61) Swayambunathan, V.; Lim, E. C. *J. Phys. Chem.* **1985**, *89*, 3960.
(62) Morozumi, T.; Anada, T.; Nakamura, H. *J. Phys. Chem. B* **2001**, *105*, 2923.
(63) Dey, J.; Haynes, J. L., III; Warner, I. M.; Chandra, A. K. *J. Phys. Chem. A* **1997**, *101*, 2271.
(64) Cotton, F. A.; Extine, M.; Gage, L. D. *Inorg. Chem.* **1978**, *17*, 172.

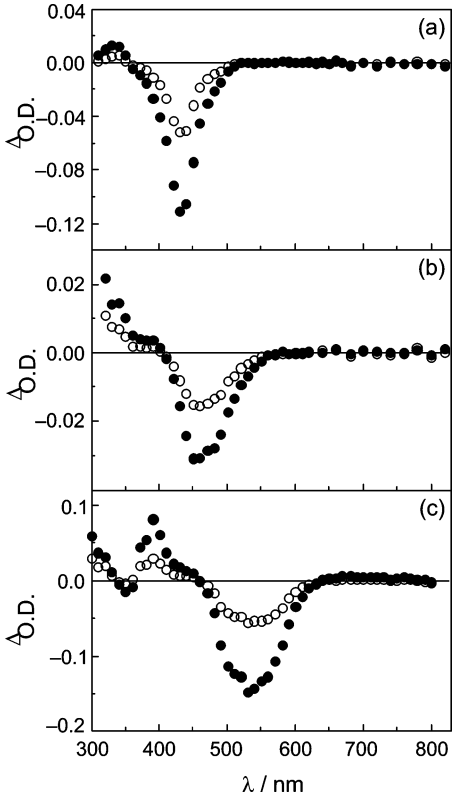

Figure 6. Transient absorption spectra of (a) 41 μM **1**, (b) 97 μM **2a**, and (c) 74 μM **4a** in THF collected (●) 2 μs and (○) 52 μs following 355 or 532 nm excitation (~5 mJ/pulse, fwhm ~ 8 ns).

complexes along this coordinate, thus resulting in a greater Stokes shift in the former. The thermally induced shift in the emission discussed above is also consistent with greater nuclear displacement in the excited state of **3** relative to the other complexes and parallels the known photophysical properties of organic molecules that possess twisted intramolecular charge transfer (TICT) excited states.[1]

Time-Resolved Measurements. The decay of the luminescence of complexes **1**−**6** takes place with $\tau < 10$ ns, however, long-lived transient absorption signals were observed from **1**−**6** following excitation with 355 or 532 nm (fwhm ~ 8 ns, 5 mJ/pulse). As shown in Figure 6, for **1**, **2a**, and **4a**, the transient absorption signals of the complexes are characterized by bleaching in the spectral region where the ground state of each complex absorbs, and there is no time-resolved absorption signal in the 550−800 nm region. In addition, positive transients were observed in the UV and near-UV region. The bleaching and positive transient signals of each complex in THF at 298 K fit a monoexponential decay with lifetimes, τ_{ta}, listed in Table 5. All transient signals returned to the baseline, and absorption measurements before and after the laser experiments did not show any sample degradation. Since the lifetimes of the transient absorption signals for the dimolybdenum complexes range from 40 to 76 μs, they cannot correspond to the emissive state.

Although time-resolved absorption signals may be due to an excited state of the complex, other processes, such as photoinduced ligand-loss or ligand rearrangement, may also give rise to transient absorption signals following excitation. However, only an excited state is able to transfer energy to a substrate, thus placing it in its excited state. The energy transfer to tetracene was observed following 532 nm (fwhm ~ 8 ns, 5 mJ/pulse) excitation of **3**. The transient absorption spectrum of 80 μM **3** in the absence and presence of 0.46 mM tetracene is shown in Figure 7. It is apparent from Figure 7 that new transient features appear at 440, 470, and 500 nm in the presence of tetracene, which are in a good agreement with the transient absorption spectrum of the $^3\pi\pi^*$ excited state of tetracene.[65,66] Since the $^3\pi\pi^*$ state of tetracene cannot be accessed directly under these experimental conditions, absorption of a 532 nm photon by **3** is followed by energy transfer to the substrate. Owing to overlap of the transient absorption signals of **3** and tetracene, detailed kinetics of the energy transfer process could not be obtained. However, the energy transfer from **3** to tetracene indicates that the transient absorption spectrum of the complex is due to an excited state of the complex. In addition, this excited state must lie above that of $^3\pi\pi^*$ of tetracene at 1.27 eV.[67] It should be noted that with the concentration of tetracene used, bimolecular energy transfer from the short-lived emissive state is not possible owing to the limiting rate of diffusion.

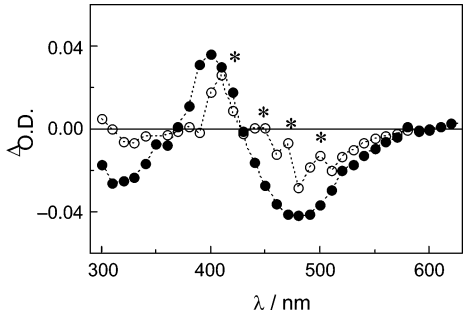

Figure 7. Transient absorption spectra of 80 μM **3** in THF in the absence (●) and presence (○) of 0.46 mM tetracene collected 2 μs following 532 nm excitation (~5 mJ/pulse, fwhm ~ 8 ns).

As discussed above, intense transient absorption signals are observed for the Mo_2 complexes in the UV and near-UV regions. It should be noted that in some cases fine structure is observed in the positive time-resolved signal, such as in **3** ($\lambda_{max} = 390$ nm), **4a** ($\lambda_{max} = 400$ nm), and **4b** ($\lambda_{max} = 360$ nm). The position of the maxima of these transients correlates well with the reported absorption spectra of the corresponding aromatic anion.[68,69] Since in the long-lived excited state the transient absorption corresponds to the reduced aryl carboxylate ligand, its identity may be assigned as the ^{3}MLCT state with electron configuration $(\delta)^1(\text{aryl } \pi^*)^1$. As will be discussed in more detail below, it is likely that the short-lived emissive state is then the ^{1}MLCT, whereas the long-lived nonemissive excited state is due to the corresponding to the ^{3}MLCT.

On the basis of the absorption, emission, electrochemical, and transient absorption data, a Jablonski diagram that describes the excited states of complexes **1**−**4** was constructed and is shown in Figure 8. As discussed above, the lowest energy emissive state is the ^{1}MLCT of each complex, with a nonemissive ^{3}MLCT at a lower energy which can be accessed from the corresponding singlet state through intersystem crossing. It should be noted that the $^1\delta\delta^*$ and $^3\delta\delta^*$ are also likely to be low-energy states. Although these states may play a role in the deactivation dynamics of the ^{1}MLCT and/or ^{3}MLCT states, they

(65) Pavlopoulos, T. G. *J. Chem. Phys.* **1972**, *56*, 227.
(66) Meyer, Y. H.; Astier, R.; Leclercq, J. M. *J. Chem. Phys.* **1972**, *56*, 801.
(67) Murov, S. L.; Carmichael, I.; Hug, G. L. *Handbook of Photochemistry*, 2nd ed.; Marcel Dekker: New York, 1993.
(68) Shida, T.; Iwata, S. *J. Am. Chem. Soc.* **1973**, *95*, 3473.
(69) Zahradnik, R.; Carsky, P. *J. Phys. Chem.* **1970**, *74*, 1240.

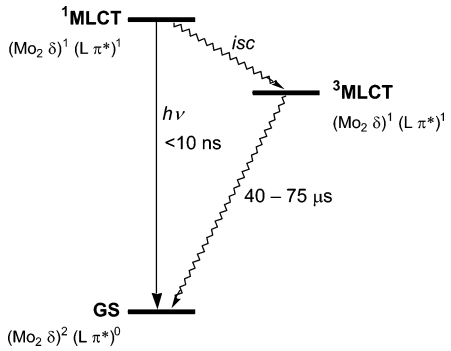

Figure 8. Jablonski diagram for the Mo_2 complexes showing the emissive ^{1}MLCT state and nonemissive long-lived ^{3}MLCT state.

are not observed and their energies remain unknown. The lifetimes of the ^{3}MLCT states of complexes **1**−**4** are 1 or 2 orders of magnitude longer than those commonly observed for ^{3}MLCT excited states of mononuclear complexes.[53] This difference may be due to a larger distance and decreased coupling between the oxidized bimetallic core and the reduced aryl ligand in the MLCT excited state of the dinuclear complexes, which are coupled through the carboxylate units. In the case of $[Ru(bpy)_3]^{2+}$, for example, the reduced aromatic ligand is directly coordinated to the metal. In addition, in $[Ru(bpy)_3]^{2+}$, it is well-known that low-lying ligand-field states play a significant role in the deactivation of the ^{3}MLCT state.[53]

Photophysical Properties of W_2 Complexes. The transitions in the absorption spectrum of **5** have been previously assigned, with a strong $W_2(\delta) \rightarrow O_2C-aryl(\pi^*)$ ^{1}MLCT absorption maximum at 592 nm and an intense shoulder at 552 nm (Table 4 and Figure 9a).[18,70] Although the presence of two peaks may be indicative of two electronic states,[18] they may also be attributed to a vibronic progression. Similar transitions were also observed in other W_2 complexes, such as $W_2(O_2C-Ph)_4(neopentyl)_2$.[70] The metal-centered $^1\delta\delta^*$ transition is weak and overlaps with the strong ^{1}MLCT transitions. Similarly, **6** also exhibits two strong ^{1}MLCT absorption bands at 598 and 645 nm as in **5**. The naphthalene π^* LUMO lies at lower energy than that of benzene, thus the ^{1}MLCT transitions in **6** are observed at lower energies than those in **5** by ∼0.17 eV.

The replacement of the Mo_2 core by W_2 has been shown to raise the energy of the δ orbital by 0.7−1.0 eV.[16,41,70−73] If the energy of $O_2C-aryl$ π^* orbitals of the aromatic carboxylate ligands is similar in the Mo_2 and W_2 complexes, then a red shift in the absorption corresponding to the ^{1}MLCT $M_2(\delta) \rightarrow O_2C-aryl(\pi^*)$ (M = Mo, W) transition would be expected in the latter relative to the former. Indeed, Table 4 shows that for **5** and **6** the lowest energy absorption maxima are shifted by 6640 (0.82 eV) and 6050 cm^{-1} (0.75 eV) relative to those in the corresponding Mo_2 complexes, **1** and **2b**, respectively.

Both **5** and **6** are weakly emissive (τ < 10 ns) with maxima at 645 and 711 nm, respectively, and their emission spectra mirror the lowest energy absorption of each complex, as shown in Figure 9a for **5**. The Stokes shifts of the W_2 complexes are significantly smaller than those of the Mo_2 systems discussed above (Table 5), indicative of a greater nuclear displacement between the ground and excited state in the Mo_2 complexes relative to **5** and **6**. As described for the Mo_2 systems, the

(70) Cayton, R. H.; Chisholm, M. H.; Huffman, J. C.; Lobkovsky, E. B. *J. Am. Chem. Soc.* **1991**, *113*, 8709.

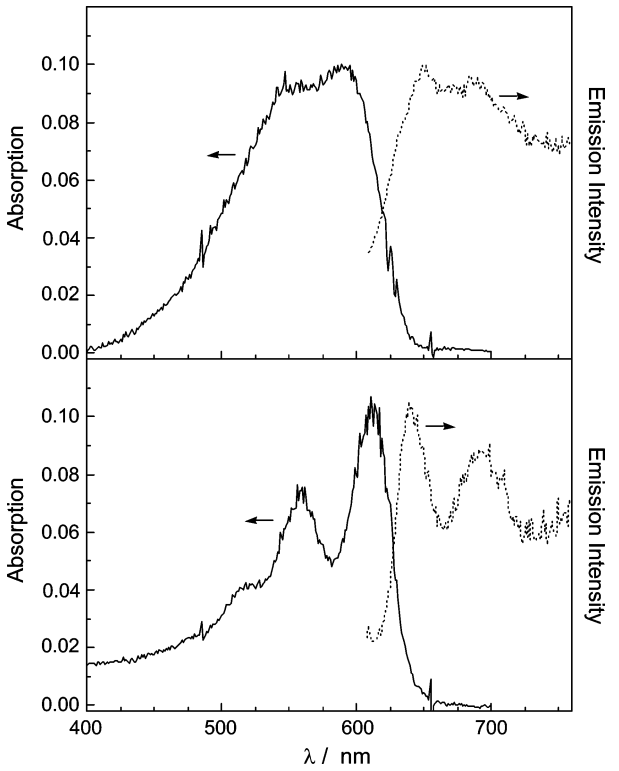

Figure 9. Emission (· · ·, λ_{exc} = 595 nm) and absorption (—) spectra of **5** at room temperature in THF (upper panel) and 77 K in 2-Me-THF (lower panel).

emission energies of **5** and **6** correlate well with the HOMO−LUMO gap obtained from electrochemical measurements. The absorption and luminescence spectra of **5** collected in 2-methyltetrahydrofuran (2-Me-THF) at 77 K are shown in Figure 9b, both of which exhibit vibronic progressions. The vibronic progression of the absorption has average $\Delta\nu$ = 1538 cm^{-1}, consistent with vibrations associated with the benzoate ligands. The luminescence resembles the mirror image of the absorption, with $\Delta\nu$ = 1219 cm^{-1}. From these observations and the analogy to the Mo_2 complexes, the emissions in **5** and **6** likely arise from the ^{1}MLCT excited state of the complexes.

The transient absorption spectra of **5** and **6** are shown in Figure 10 and are characterized by intense bleaching of the ground-state absorption in the 500−700 nm region and a broad absorption signal from 300 to 500 nm. The lifetimes of the photogenerated transients of **5** and **6** were measured to be ∼58 and ∼75 ns, respectively. Although the lifetimes are only approximate owing to the instrument response with fwhm ∼ 20 ns, they are both greater than the emission lifetimes of each complex (<10 ns). As is the case in the Mo_2 complexes, the longer-lived nonemissive excited state may be ascribed to the ^{3}MLCT excited state of the W_2 complexes. The $\sim10^3$ shorter lifetime of the ^{3}MLCT of the W_2 systems relative to those of Mo_2 can be explained by the greater spin−orbit coupling (heavy atom effect) in the former compared to the latter, resulting in faster intersystem crossing from the triplet excited state to the singlet ground state (Figure 8). In addition to increased spin−orbit coupling, based on the energy of the emissive ^{1}MLCT states, the energy gap between the ground state and the ^{3}MLCT in **5** is approximately 3500 cm^{-1} smaller relative to that in **1** and for compound **6**, 2100 cm^{-1} compared to that for **2b**. Such shift is predicted by the energy gap law to result in greater

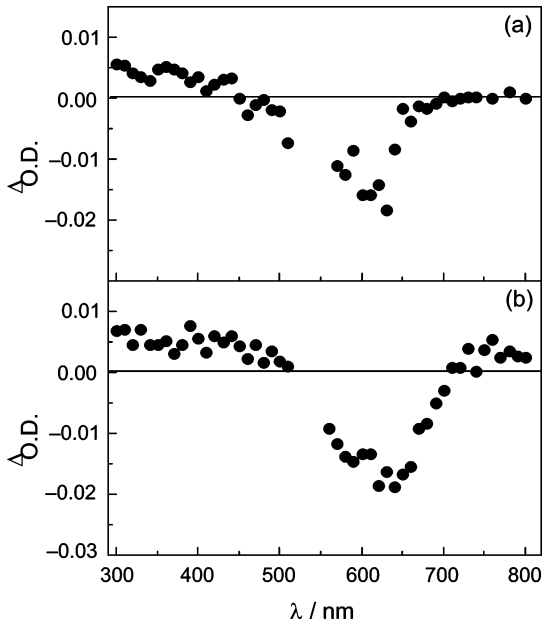

Figure 10. Transient absorption spectra of (a) 16 μM **5** and (b) 15 μM **6** in THF collected 10 ns following 532 nm excitation (~5 mJ/pulse, fwhm ~ 8 ns).

nonradiative deactivation in the W_2 complexes relative to the corresponding Mo_2 systems.[74] The presence of other low-lying states which may also result in deactivation of the ^{3}MLCT excited state cannot be ruled out at this time.

Concluding Remarks

To our knowledge, this work represents the first example of quadruply bonded complexes with emissive ^{1}MLCT and nonemissive ^{3}MLCT excited states. Comparisons can be made between the photophysical properties of these bimetallic complexes with those of $[Ru(bpy)_3]^{2+}$. Of particular note is that the lifetimes of the ^{3}MLCT excited states of the $Mo_2(O_2C-Ar)_4$ compounds (40−76 μs) are significantly longer than that of $[Ru(bpy)_3]^{2+}$ (620 ns in H_2O).[2,3] As discussed above, the ^{3}MLCT lifetimes for the tungsten compounds are significantly shorter due to increased spin−orbit coupling and nonradiative deactivation resulting from a lower energy excited state. An important difference between the ^{3}MLCT excited state of $[Ru(bpy)_3]^{2+}$ and that of the $Mo_2(O_2C-Ar)_4$ compounds is that the former is emissive, whereas the latter is not. In the $Mo_2(O_2C-Ar)_4$ complexes, the short-lived luminescence is believed to originate from the ^{1}MLCT excited state. The photophysical properties of the present systems parallel those of aromatic organic molecules with fluorescent $^1\pi\pi^*$ and nonemissive $^3\pi\pi^*$ excited states. In this regard, these quadruply bonded complexes may be viewed as metal-mediated organics, where the introduction of the M_2 δ orbital in conjugation with organic π-system affords the opportunity to tune the energies of the ^{1}MLCT and ^{3}MLCT excited states.

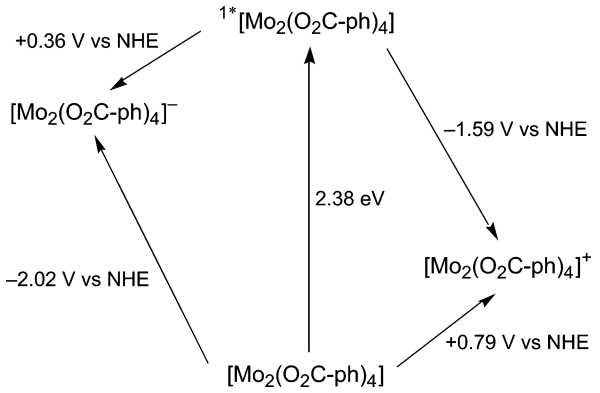

Figure 11. Latimer diagram of the emissive ^{1}MLCT excited state of $Mo_2(O_2C-ph)_4$.

A representative Latimer diagram is shown in Figure 11 for $Mo_2(O_2C\text{-}ph)_4$ (**1**), showing that the emissive ^{1}MLCT excited state is expected to be a strong reducing agent, $E_{1/2}(\mathbf{1}^{+/*}) = -1.59$ V vs NHE, and a modest oxidizing agent, $E_{1/2}(\mathbf{1}^{*/-}) = +0.36$ V vs NHE, compared to the ^{3}MLCT of $[Ru(bpy)_3]^{2+}$ with $E_{1/2}(Ru^{3+/2+*}) = -0.83$ V vs NHE and $E_{1/2}(Ru^{2+*/+}) = +0.79$ V vs NHE. Similar excited-state redox potentials can be calculated for complexes **2**−**4**. Since the energy of the ^{3}MLCT excited state of $Mo_2(O_2C-9\text{-}an)_4$ (**3**) is known to be $E_{00} > 1.27$ eV from the energy transfer experiment, the excited-state oxidation and reduction potentials can be estimated to be $E_{1/2}(\mathbf{3}^{+/*}) < -0.28$ V vs NHE and $E_{1/2}(\mathbf{3}^{*/-}) > -0.19$ V vs NHE, respectively. Therefore, the long-lived excited states of the Mo_2 series of complexes are also likely to be good reducing agents. For the W_2 complex **5**, with ^{1}MLCT $E_{00} = 1.94$ eV, $E_{1/2}(\mathbf{5}^{+/*}) = -1.67$ V vs NHE, and $E_{1/2}(\mathbf{5}^{*/-}) = -0.18$ V vs NHE, the emissive excited state of the complex is expected to be a good reducing agent, but substrate oxidation would be thermodynamically unfavorable.

Additional studies aimed at investigating the early processes of excited-state evolution in the $Mo_2(O_2C-Ar)_4$ complexes, using femtosecond time-resolved techniques, are currently underway.

Acknowledgment. M.H.C. thanks the National Science Foundation for financial support (CHE-0131832), and the Ohio Supercomputer Center for computing support. C.T. thanks the National Institutes of Health (RO1 GM64040-01). The authors thank Prof. Christopher Hadad for help with the calculations, and Patricia Bradley for aid with some photophysical measurements.

Supporting Information Available: A complete list of bond parameters and the CIF file for the crystal structure of $[Mo_2(O_2C\text{-}9\text{-}an)_4]\bullet(C_4H_8O)_2$ (**3**). Transient absorption spectra of **2b** and **4b**. Complete list of authors for ref 26. This material is available free of charge via the Internet at http://pubs.acs.org.

JA055136H

(71) Bursten, B. E.; Chisholm, M. H.; Clark, R. J. H.; Firth, S.; Hadad, C. M.; Macintosh, A. M.; Wilson, P. J.; Woodward, P. M.; Zaleski, J. M. *J. Am. Chem. Soc.* **2002**, *124*, 3050.
(72) Chisholm, M. H.; Patmore, N. J. *Inorg. Chim. Acta* **2004**, *357*, 3877.
(73) Chisholm, M. H.; Clark, R. J. H.; Gallucci, J.; Hadad, C. M.; Patmore, N. J. *J. Am. Chem. Soc.* **2004**, *126*, 8303.
(74) Caspar, J. V.; Meyer, T. J. *J. Phys. Chem.* **1983**, *87*, 952.